CNS Connectivity: The MR Connectome

An Vu   **jvu@umn.edu**

- Characterizing connectomes benefit from high quality, high resolution MRI
- Going to high field enables higher resolution MRI but is challenging
- Some challenges include: motion sensitivity, B_1^+ inhomogeneity, and SAR
- Techniques to mitigate these challenges and resulting data are described

What are we trying to learn from the Human Connectome Project?

Target Audience:
Clinicians and researchers interested in high resolution, slice accelerated functional and diffusion MRI (fMRI/dMRI).

Outcome:
After the course, learners will be able to optimize their fMRI/dMRI acquisition protocol to acquire higher quality, higher resolution, whole brain images for exquisite characterization of human connectomes.

Purpose:
Mapping the human connectome in healthy adults for the Human Connectome Project (HCP) benefits from high quality, high resolution, multiband (MB)-accelerated whole brain fMRI and dMRI [1-3]. Higher field strengths provide higher SNR and the opportunity to acquire at higher resolution [4], however, this comes at the cost of increased motion sensitivity [5] (due to required in-plane phase encoding acceleration), B_1^+ inhomogeneity (resulting in signal loss in cerebellar and temporal lobe regions) and SAR (limiting our ability reduce TR or accelerate). This course describes the some of the steps the HCP has taken to mitigate these costs and facilitate high resolution, whole brain fMRI/dMRI at 3 and 7T.

Methods:

To enable high slice and in-plane acceleration data shown (unless otherwise stated) were acquired using a 32 channel receive and quadrature transmit coil (Nova Medical, Wilmington, MA) on a Siemens Magnetom 7T body gradient system (70mT/m, 200mT/m/s).

Reducing motion sensitivity with the GRE FLASH reference

To evaluate motion sensitivity of reference scans in in-plane + slice accelerated imaging, high resolution, whole brain gradient-echo EPI was acquired at 1.5, 1.25 and 0.9 mm isotropic resolutions. For repeatability testing, each resolution was acquired three times per reference scan type: SEG ref (standard segmented EPI), SS ref (single shot EPI), GRE ref (GRE FLASH). These reference scans were used for in-plane unaliasing while single-band in-plane under-sampled scans were used for MB slice unaliasing. In-plane (GRAPPA) and slice (multiband, MB) acceleration factors were both 3 with a ¼ FOV shift in the PE direction using blipped-

CAIPIRINHA [6]. Echo spacings were minimized and TE was ~19ms requiring 7/8, 6/8, and 5/8 partial Fourier; 1300, 1900, and 3600ms TR for each resolution respectively. Z-coverage was ~135mm. For the 0.9mm data, this required 150 slices and a custom modification to both pulse sequence and reconstruction code to overcome the vendor specific 128-slice limit.

Reducing B_1^+ inhomogeneity with dielectric pads

To enhance the transmit B_1^+ in the cerebellum and temporal lobes, high permittivity dielectric pads, consisting of a suspension of calcium titanate powder ($_r \approx 110$) were placed under the neck and on both sides of the head [7]. For comparison, the subject was scanned with and without pads.

Reducing SAR and its overestimation

SAR reduction in dMRI was achieved using low SAR fat suppression with 5ms excitation and 10ms refocusing RF pulses [8]. Peak power and online (vendor specific) SAR measurement error/overestimation were reduced using ~2ms time shifted MB RF pulses in dMRI [9] and MB RF phase optimization in fMRI [10]. SAR measurement error can become significant and result in prematurely aborted scans in high resolution, slice accelerated imaging due to the MB RF pulse modulations being fast relative to the impulse response function of the SAR monitor. This measurement error was empirically calculated for various MB factors and slice spacings by comparing the log files of the system-measured 10 second average forward power to the pre-calculated expected forward power. The original, standard excitation RF pulses were then compared in Matlab (Natick, MA) to versions filtered by impulse response functions of various decay rates (τ; Fig 4C). The τ that best matched the empirical SAR measurement error was 25 μs. The SAR "error factor" for several MB factors and slice spacings was calculated (with $\tau = 25$ μs) as the ratio of filtered to original RF pulse power integrals (Fig 5). Phase optimized [10] and time-shifted [9] (1280ms shift for 5120ms pulses) MB RF pulses were simulated and evaluated regarding their ability to minimize SAR measurement errors.

Results and Discussion:
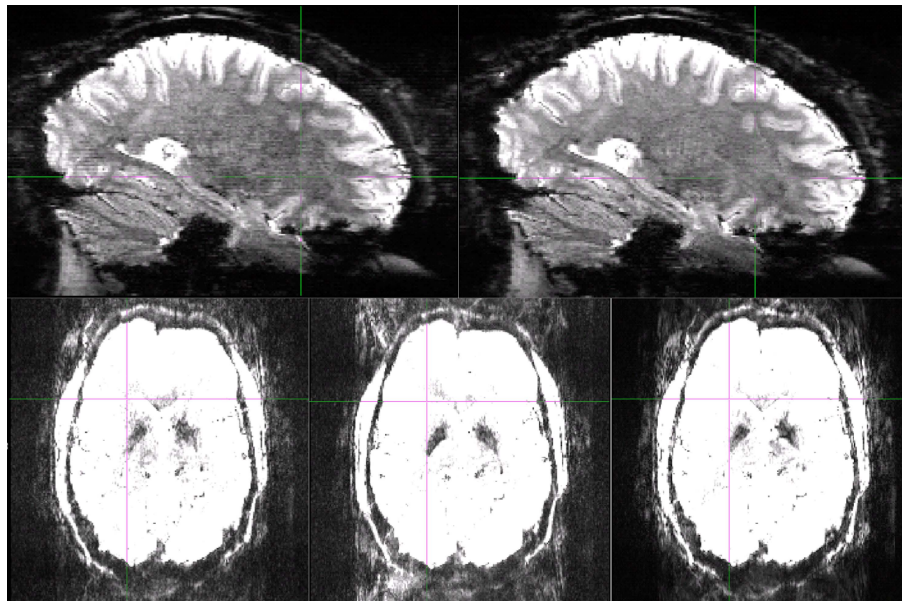
Figure 1: Image quality from a still subject using various reference scans at 0.9mm
Sagittal slices (top row): SEG ref shows dark/bright pattern in alternating slices (left), GRE ref improves image quality substantially (right). Axial slices windowed to view noise (bottom row): SEG ref (left), SS ref adds additional ghosting (middle), GRE ref greatly reduces noise (right).
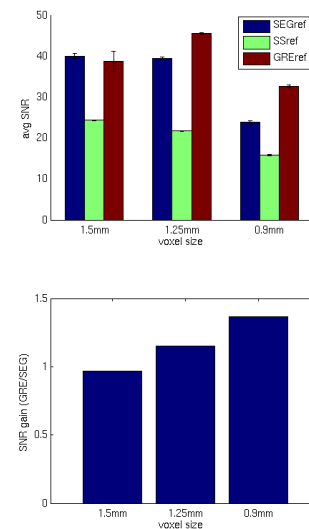
Figure 2: SNR comparison
Average SNR is worst for SS ref at all resolutions (top). GRE ref has largest improvements for highest spatial resolutions (bottom)
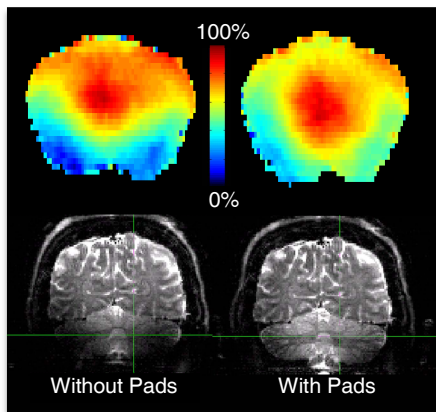

Figure 3: Effects of dielectric pads
AFI flip angle maps (top) and 7T b=0 in-vivo images (bottom)

Fig 1 shows that even in the presence of minimal head motion, in-plane acceleration combined with slice accelerated EPI can result in dark/bright alternating slice intensities (or "horizontal stripes"; top left) as well as increased ghosting and reconstruction noise (bottom left). Although the SS ref provided shorter reference scan times, it resulted in significantly increased noise and ghost levels for the GRAPPA3xMB3 acquisition (Fig 1, bottom middle). Use of the GRE ref significantly improved image quality (contrast homogeneity), while reducing both the dark/bright slice artifact and reconstruction noise. Average SNR across the brain in three separate acquisitions also showed significant improvements at higher spatial resolutions with the GRE ref (Fig 2, top). The improvement over a standard SEG ref increased with spatial resolution (Fig 2, bottom), reaching a factor of 140% for the 0.9mm (equivalent to two averages of SEG ref data).

Low SAR fat saturation and time shifting enabled an MB acceleration factor of 2 and a TR of 7000ms without compromising the slice bandwidth or profile. Without these, TR and acquisition time would have increased by at least 70% (~32 mins) to stay within SAR limits. Figure 3 shows the effect of the dielectric pads on B_1^+ (AFI [11]; top row) and image quality (bottom row). Without the pads, flip angles in the cerebellum are ~1/4th of the nominal flip angle resulting in

low signal/tissue contrast in the cerebellum. With the pads, flip angles in cerebellar regions increase on average by a factor of 2 corresponding to a 4-fold increase in image SNR relative to without the pads.
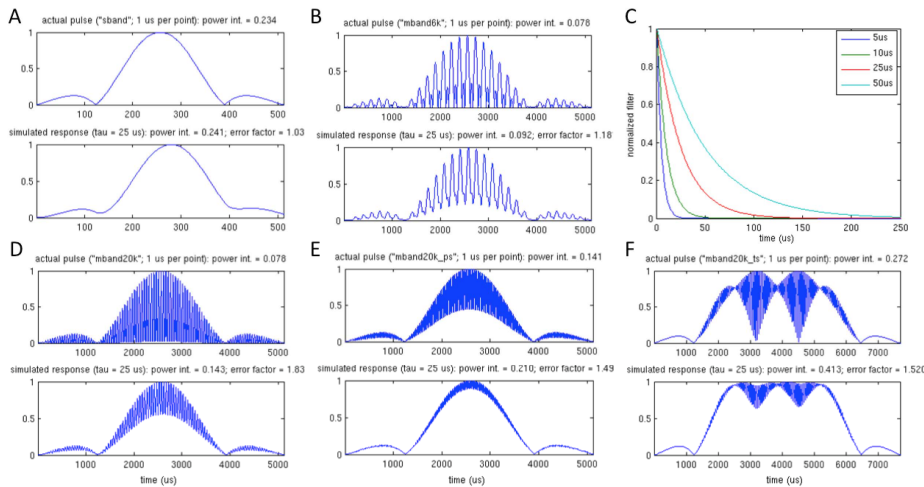
Figure 4: Original and filtered MB RF pulses. A) Original single band pulse (top), filtered pulse (bottom). B) MB=3, 6kHz slice spacing. C) Impulse response functions for various decay rates. D) MB=3, 20kHz slice spacing. E) Same as D with phase optimized pulses. F) Same as D with time-shifted pulses.
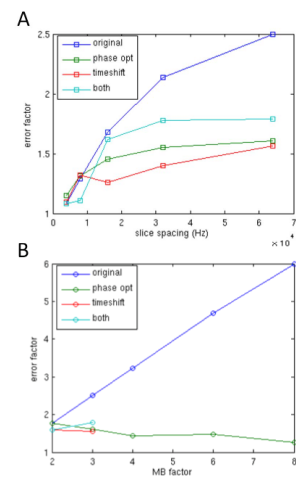
Figure 5: SAR error factors
A) As a function of slice spacing
B) As a function of MB factor
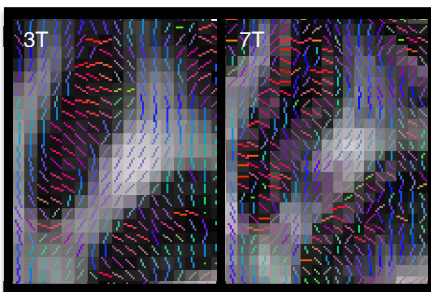
Figure 6: Enhanced layer specific cortical diffusion information at 7T in-vivo.
3T (left) 7T (right) Dark bands of low FA at the gray-white matter boundaries accompanied by fibers turning sharply into cortex become visible at 7T (coronal slice).

Fig. 4A compares the original single band RF excitation pulse (top) to the filtered RF pulse (bottom). In this case, SAR measurement error is negligible. Fig. 4B shows the case for MB=3 with an MB slice spacing of 6kHz. Here, the filtered version does not capture the deep troughs resulting in an SAR error factor of 1.18 (or 18% over-measurement). Increasing the MB slice spacing to 20kHz (Fig 4D) for larger brain coverage amplifies the error factor to 1.83. With phase optimization (Fig 4E) or time-shifting (Fig 4F), the SAR error factor is reduced to ~1.5 (reducing over-measurement by almost 40%). Fig 5A shows that the error factor (with MB=3) increases sub-linearly (up to a factor of ~2.5) with increasing slice spacing. Figure 5B shows that the error factor (with slice spacing = 64kz; whole brain) increases linearly with MB factor. Time-shifting was not calculated for MB>3 since RF pulses would be greater than 8ms. In both cases, the addition of phase optimization and time-shifting significantly reduced error factors, with larger reductions to be gained at larger slice spacings and higher MB factors. For MB=2, only time-shifting provides a reduction in the error factor. Nevertheless, this is still important for high field where sequences, like spin-echo diffusion MRI at 7T, tend to run near SAR limits, whereby preventing any acceleration.

Figure 6 compares a zoomed in coronal view of the principle diffusion from both the HCP 3T (left) and 7T (right). The improvement in spatial resolution at 7T enables visualization of the white matter tracts making sharp turns into cortex, which are much harder to see in the 3T data.

The 7T data also provides excellent detail including layer specific regions of low FA along the gray-white matter boarders previously only shown in high-resolution human data ex-vivo [12,13].

Conclusion:

Careful optimization of motion robust reference scans, B_1^+ homogeneity, and SAR at high field allow for high quality, high resolution, whole brain imaging. With motion prone subjects and/or higher spatial resolutions (<1.25mm) a more robust reference scan like a GRE ref is necessary for clean images. Once clean higher spatial resolution images are achieved, visualization of features such as cortical layer specific anisotropy and FA previously only seen in ex-vivo human studies is possible and will certainly be advantageous when characterizing dense human connectomes.

It should be noted that while high quality high, SNR diffusion data can be generated at 7T, the HCP 3T acquisitions benefit from higher gradient strengths (100 mT/m) and relaxed SAR limits, putting the 7T acquisitions at a significant disadvantage. Improvements in gradient performance at 7T, along with parallel transmit technology to reduce SAR [14], will only improve the 7T data further. Future work for the HCP will involve evaluating whether there is benefit in combining information from 3T and 7T fMRI/dMRI data.

References:

[1] Uğurbil, K., et al. "Pushing Spatial and Temporal Resolution for Functional and Diffusion Mri in the Human Connectome Project." *Neuroimage* 80 (2013): 80-104.
[2] Van Essen, D. C., et al. "The Wu-Minn Human Connectome Project: An Overview." *Neuroimage* 80 (2013): 62-79.
[3] Sotiropoulos, S. N., et al. "Advances in Diffusion Mri Acquisition and Processing in the Human Connectome Project." *Neuroimage* 80 (2013): 125-43.
[4] Yacoub, E., et al. "Imaging Brain Function in Humans at 7 Tesla." *Magn Reson Med* 45.4 (2001): 588-94.
[5] Moeller, S., et al. "Fmri with 16 Fold Reduction Using Multibanded Multislice Sampling." *Proc. Int. Soc. Magn. Reson. Med.*2008 2366 Vol. 16.
[6] Setsompop, K., et al. "Blipped-Controlled Aliasing in Parallel Imaging for Simultaneous Multislice Echo Planar Imaging with Reduced G-Factor Penalty." *Magn Reson Med* 67.5 (2012): 1210-24.
[7] Teeuwisse, W. M., W. M. Brink, and A. G. Webb. "Quantitative Assessment of the Effects of High-Permittivity Pads in 7 Tesla Mri of the Brain." *Magn Reson Med* 67.5 (2012): 1285-93.
[8] Ivanov, D., et al. "A Simple Low-Sar Technique for Chemical-Shift Selection with High-Field Spin-Echo Imaging." *Magn Reson Med* 64.2 (2010): 319-26.
[9] Auerbach, E. J., et al. "Multiband Accelerated Spin-Echo Echo Planar Imaging with Reduced Peak Rf Power Using Time-Shifted Rf Pulses." *Magn Reson Med* 69.5 (2013): 1261-7.
[10] Wong, E. "Optimized Phase Schedules for Minimizing Peak Rf Power in Simultaneous Multi-Slice Rf Excitation Pulses." *Proc. Int. Soc. Magn. Reson. Med*. 2012. 2209.
[11] Yarnykh, V. L. "Actual Flip-Angle Imaging in the Pulsed Steady State: A Method for Rapid Three-

Dimensional Mapping of the Transmitted Radiofrequency Field." *Magn Reson Med* 57.1 (2007): 192-200.

[12] Miller, K. L., et al. "Diffusion Imaging of Whole, Post-Mortem Human Brains on a Clinical Mri Scanner." *Neuroimage* 57.1 (2011): 167-81.

[13] Leuze, C. W., et al. "Layer-Specific Intracortical Connectivity Revealed with Diffusion Mri." *Cereb Cortex* (2012).

[14] Wu, X., et al. "Simultaneous Multislice Multiband Parallel Radiofrequency Excitation with Independent Slice-Specific Transmit B1 Homogenization." *Magn Reson Med* (2013).